RSC Advances

ROYAL SOCIETY OF CHEMISTRY

www.rsc.org/advances

Preparation and characterization of PbO$_2$ electrode modified with Polyvinyl alcohol (PVA)

Xiaoliang Li, Hao Xu*,Wei Yan*

Department of Environmental Science and Engineering, State Key Laboratory of Multiphase flow

in Power Engineering, Xi'an Jiaotong University, Xi'an, 710049, China

*Corresponding authors:

E-mail: yanwei@xjtu.edu.cn; xuhao@xjtu.edu.cn

Tel.: +86-15829780706; fax: +86-29-82664731.

Abstract: A novel PbO_2 electrode was successfully synthesized with polyvinyl alcohol (PVA) modification through electro-deposition technology. The morphology and crystalline structure of the electrodes were characterized by SEM and XRD, respectively. In addition, X-ray photoelectron spectroscopy (XPS), cyclic voltammetry (CV), electrochemical impedance spectroscopy (EIS) and accelerated life test stability were also carried out to analyze the chemical state, electrochemical performances and stability of electrodes. The results showed that PVA could refine the grain size and increase oxygen evolution potential (OEP). After PVA modification, the predominant phase of PbO_2 electrodes were unchanged and all were pure β-PbO_2. Besides, for modified electrodes, the electrode film impedance reduced and the proportion of adsorbed hydroxyl oxygen (O_{ad}) on the electrode increased implying the fast charge transfer and excellent degradation efficiency for organics. In the process of dye oxidation, the PbO_2-2.0 vt% electrode showed the highest electrocatalytic activity for ARG degradation due to its highest OEP and massive O_{ad}. Moreover, the accelerated service life tests revealed that PbO_2-2.0 vt% electrode exhibited the highest stability and the accelerated service life was 329.5 h, which was more than 3 times longer than that of PbO_2-0 vt% electrode (96 h).

Keywords: PbO_2 electrode; modification; PVA; electrocatalytic activity; stability

1. Introduction

Electro-catalytic oxidation technology (EOT) is becoming an attractive approach for

wastewater treatment on account of its high efficiency, easy control, versatility, and environmental friendliness [1, 2]. In the process of electro-catalytic oxidation, electrode is the core which strongly affects the efficiency of organic pollutants oxidation [3, 4]. Therefore, it is very important to develop a novel electrode material with high catalytic activity and stability. So far, many kinds of electrodes have been studied, including graphite, Pt, boron doped diamond (BDD), RuO_2, IrO_2, SnO_2 and PbO_2, etc. [5-11]. Among these electrodes, Ti/PbO_2 was considered to be a more promising and attractive electrode in wastewater treatment process due to its low cost, ease of preparation, high OEP and long service lifetime [12-14]. However, the fragile PbO_2 coating is easily to peel off and dissolved in the process of electrolysis, which could lead to the reduction of the electrocatalytic activity and stability of electrode as well as cause the secondary water pollution [15-17]. Hence, it is necessary to modify the PbO_2 electrode to meet the standards of industrial electrodes.

Doping is a frequently-used and effective way to modify PbO_2 electrode for improving its performance. Lots of foreign materials have been adopted, such as metallic element (Bi [18], Co [19], Fe [20], Ce [21], Cu [22]), non-metallic element (F [19, 23, 24]), redox ion ($[Fe(CN)_6]^{3-}$ [13]) and compounds (TiO_2 [25], clay [26], carbon nanotubes [27], fluorine resin (FR) [15], Polypyrrole (PPy) [28] and polytetrafluoroethylene (PTFE) [29]), etc. The results show that the modified PbO_2 electrode exhibits excellent electrocatalytic ability and stable performance. Alcohols can also be used as modifiers for electrodes. Alcohols addition can affect the rate of metal ions migration and crystallization. Recently，to the best of my knowledge, there are two reports about the alcohols

modified PbO$_2$ electrode. Xu et al.[30] studied the effect of ethylene glycol (EG) modification on the electrochemical properties of PbO$_2$ electrode. Yang et al.[31] reported that the PbO$_2$ electrode was modified with polyethylene glycol (PEG). Based on the two reports, it could be concluded that after the modification by alcohols, the electrodes both have excellent electro-catalytic activity and stability.

Polyvinyl alcohol (PVA) is an important chemical raw material and has been widely used for many applications including textile, paper, adhesives, adhesives, and so on [32]. In addition, PVA is also a kind of nonionic surfactant and used in the production of emulsifier and dispersant. Adding proper amount of surfactant into the electroplating solution can effectively improve the morphology of the coating and the performance of the electrode [33]. Meanwhile, PVA is nontoxic to organisms and is the only known xenobiotic carbon chain polymer to biodegrade at high molecular masses [34]. Therefore, using PVP to modify the PbO$_2$ electrode would be very interesting and promising. But at present, to the best of our knowledge, studies of polyvinyl alcohol (PVA)-doped PbO$_2$ electrode have not been previously reported.

Therefore, in the present work, polyvinyl alcohol (PVA) was adopted to modify the PbO$_2$ electrode by electrochemical deposition. The morphology, crystalline structure and electrochemical performances were characterized. Acid red G (ARG, C$_{18}$H$_{13}$N$_3$Na$_2$O$_8$S$_2$, CAS number: 3734-67-6) was chosen as the model pollutant for electro-catalytic oxidation to evaluate electrochemical activity of the electrodes. Besides, Pb element leaching of PbO$_2$ electrodes was studied during electrolysis process to evaluate the safety. Furthermore, the accelerated life test was also carried

out to assess its stability.

2. Experimental

2.1. Materials and reagents

All chemicals (analytical grade) were obtained from Sinopharm Chemical Reagent Xi'an Co., Ltd and used without further purification. Pure (>99.6%) titanium plates with 0.5 mm thickness were purchased from BaoTi Co., Ltd. and used as the substrate. Deionized water with conductance of 18 MΩ cm was was prepared by an EPED-40TF water purification laboratory system (Yipuyida Technology development Ltd., Nanjing, China).

2.2. Electrode preparation

Ti plates (3 cm×5 cm×0.5 mm) were used as the electrode substrate. The pre-treatment of Ti plates and the fabrication of the Sb-SnO$_2$ inner layer (brush coating-thermal deposition method) were carried out according to our previous work [13, 22]. The surface β-PbO$_2$ layer was deposited on the Ti/Sb–SnO$_2$ surface through the electrochemical deposition method. The electro-deposition solution contained 0.5 mol·L^{-1} Pb(NO$_3$)$_2$, 0.1 mol·L^{-1} Cu(NO$_3$)$_2$, 0.01 mol·L^{-1} NaF, 0.1 mol·L^{-1} HNO$_3$ and the solution dissolved different volume fractions of PVA (0 vt%, 1.0 vt%, 2.0 vt% and 5.0 vt%, marked as PbO$_2$-0 vt%, PbO$_2$-1.0 vt%, PbO$_2$-2.0 vt% and PbO$_2$-5.0 vt%, respectively). The pretreated Ti/Sb–SnO$_2$ was used as anode in electro-deposition solution (65 °C) for 120 min under the current density of 10 mA·cm^{-1}. The copper sheet with the same size was adopted as the counter cathode. The average amount of

PbO$_2$ coating on the electrode surface is 91.6 ± 0.3 mg·cm^{-2} exclusive of PbO$_2$-5.0 vt%

(PbO$_2$-5.0 vt%: 83.5 mg·cm^{-2}).

PVA (Type 1799) was dissolved as follows: Firstly, adding 2 g PVA slowly to a beaker

filled with 100 mL deionized water (25 °C). The beaker would be sealed which could

reduce the water evaporation. Secondly, the solution was fully swollen at room

temperature (25 °C) for 12 h and performed at a heating rate of 5 °C · min^{-1} from 25

°C to 90 °C. Thirdly, the solution was kept at 90 °C for 3 h, until the tiny particles in

the solution disappeared. Finally, the solution was filtered through 80 mesh of

stainless steel to remove impurities and prepared for PbO$_2$ electrodes modification.

2.3. Characterization analysis

The morphology and crystal structure of PbO$_2$ electrodes are analyzed by scanning

electron microscopy (SEM, JEOL, JSM-6390A) and X'pert PRO MRD diffractometer

(XRD, PAN alytical, Holland) using Cu K$_\alpha$ source (λ = 0.15416 nm). The chemical

states of O on the electrodes were analyzed by the X-ray photoelectron spectroscopy

(XPS) performed on Axis Ultra spectrometer (Al K$_\alpha$ radiation; 1486.6 eV). Binding

energy of the C 1s peak (284.8 eV) was used as the reference for calibration.

Electrochemical properties were tested on the CHI660D electrochemical workstation

(Shanghai Chenhua Instrument Co. Ltd., China) in a standard three-electrode cell (25

°C). The fresh PbO$_2$ electrodes were served as the working electrode. Copper sheets

were acted as the counter electrode and Ag/AgCl (sat KCl) was acted as the reference

electrode. The electrolyte was 0.5 mol·L^{-1} Na$_2$SO$_4$ solution. Cyclic voltammetry (CV)

measurements were performed between 0 and 2.5 V with a sweep rate of 50 mV·s^{-1}.

Electrochemical impedance spectroscopy (EIS) measurements were carried out in a range of 10^5 Hz to 0.1 Hz at a potential of 0 V (vs. Ag/AgCl) with a sine wave of 5 mV amplitude.

The accelerated lifetime test was carried out at an anode current density of 500 mA·cm^{-2} using an electrochemical workstation (LK3000A, Tianjin Lanlike, China). The electrolyte was 3 mol·L^{-1} H$_2$SO$_4$ (35 °C ± 2 °C). The working electrode was considered as deactivation when the cell voltage reached to 10 V.

2.4. Electro-catalytic oxidation of ARG

Electro-catalytic oxidation of ARG was conducted in an undivided electrolytic cell under constant current density of 15 mA·cm^{-2} equipped with a magnetic stirrer. The volume of dye solution was 200 mL and the initial ARG concentration was 100 mg·L^{-1}. 0.1 mol·L^{-1} Na$_2$SO$_4$ was used as the supporting electrolyte. The PbO$_2$ anodes have an area of 18 cm^2 and copper sheet with the same area was used as the cathode. The gap between the electrodes was 1 cm. Electrolysis were carried out at room temperature for 120 min and the liquid samples were withdrawn from the electrolytic cell every 15 min. The dye concentrations were measured by UV-Vis absorption (Agilent 8453, Agilent) at the characteristic wavelengths of 505 nm and COD values (mg·L^{-1}) of the samples were determined by CSB/COD Reactor (ET 125 SC). The decolorization rate (η_{ARG}) and COD removal rate (η_{COD}) in electrochemical oxidation could be calculated as follows:

$$\eta_{ARG} = \frac{A_0 - A_t}{A_0} \times 100\% \qquad (1)$$

Where A_0 and A_t are the absorbance value in 505 nm of initial sample and

electrolysis at the given times t, respectively.

$$\eta_{COD} = \frac{COD_0 \cdot COD_t}{COD_0} \times 100\% \qquad (2)$$

Where COD_0 and COD_t are the initial COD concentration and COD concentration value at given time t, respectively.

The instantaneous current efficiency (ICE) and energy consumption (E_p) were calculated as follows:

$$ICE = \frac{(COD_{t_1} - COD_{t_2})}{8I(t_1 - t_2)} FV \qquad (3)$$

$$E_p = \frac{UIt}{(COD_{t_1} - COD_{t_2})V} \qquad (4)$$

Where COD_{t_1} and COD_{t_2} are the chemical oxygen demand at times t_1 and t_2, respectively, I is the current (A), F is the Faraday constant (96487 C·mol^{-1}), U is the cell voltage (V) and V is the volume of the electrolyte (L).

In order to evaluate the safety performance of the PbO$_2$ electrode in the electrolysis process. The fresh prepared electrode was electrolyzed at 15 mA·cm^{-2} for 120 min in 0.1 mol·L^{-1} Na$_2$SO$_4$ solution. The concentration of Pb element dissolved in electrolyte (No coating detachment was found) was analyzed by inductively coupled plasma atomic emission spectroscopy (ICP-AES, Shimadzu, Japan).

3. Results and discussion

3.1. Surface morphological analysis of PbO$_2$ electrodes

Fig. 1 shows the SEM images of the PbO$_2$ electrodes modified with different PVA volume fractions. From Fig. 1a, it could be observed that the PbO$_2$-0 vt% electrode showed typical pyramid structure (Octahedral crystals) with different sizes on the

surface. The electrode surface was relatively rough, and there were a number of micro

holes distributed on the surface of the coating. The PbO_2 grains were randomly

arranged and there were not obvious crystal orientation. This structure could easily

lead to the infiltration of the electrolyte into the coating, reducing the stability of the

electrode [35]. In addition, the O_2 generated by electrolysis of water would be released

from the micro holes and furtherly damaged the coating. As shown in Fig. 1b-1d, it

could be seen that after PVA adding into the deposition solution, the modified PbO_2

electrode still had the pyramid structure, but it was ordered and uniform compared

with unmodified electrode. With the increase of the PVA doping amount, the particles

of the electrode surface became smaller and smoother. The reasons could be explained

as follows: Firstly, the surface tension of the plating solution could be reduced by the

addition of surfactants (PVA), making the coating smooth and compact. Secondly,

PbO_2 crystal nucleus would be coated by PVA molecule and inhibited the growth and

aggregation of PbO_2 grains. Therefore, the particle size of PbO_2 crystals decreased.

Thirdly, the addition of PVA increased the viscosity of electroplating solution,

reducing the migration rate of Pb ions and making the current density distribute on the

electrode uniformly. Therefore, the electrode coating became compacted and smooth.

The special structure could suppress the infiltration of the electrolyte into the coating

layer and prolong the service life of the electrode.

3.2. Structure of PbO_2 electrodes

The XRD patterns of the PbO_2 electrodes are shown in Fig. 2. For PbO_2-0 vt%

electrode, the crystal structure is pure β-PbO_2 and the main diffraction peaks at 25.4°,

$32.0°$, $36.2°$ and $49.0°$ were assigned to the (110), (101), (200) and (211) crystal faces, respectively. After PVA addition, the crystalline orientation of the electrodes did not change greatly and the predominant phases were still β-PbO_2. However, the diffraction intensities of (101) and (211) planes for PbO_2-1.0 vt% and PbO_2-2.0 vt% increased significantly, indicating that the preferred orientation along the (101) and (211) directions. In addition, the diffraction intensities of (110) and (200) planes decreased. Moreover, when the PVA volume fraction increased to 2.0 vt%, the peak of (220) plane disappeared. This phenomenon could be account for the different adsorption and encapsulation of PVA on the different crystal surfaces. The planes of (110), (200) and (220) were suppressed and the planes of (101) and (211) were preferential growth. However, when the PVA volume fraction increased to 5.0 vt%, the intensities of diffraction peaks were all weak compared with other electrodes. After calculated by Debye-Scherrer formula, it could be seen that the average grain sizes of PbO_2 crystals decreased with the addition of PVA (Tab. 1). The average grain sizes of PbO_2 crystals were 21.20 nm, 20.91 nm, 19.37 nm and 19.13 nm, respectively, which was consistent with SEM results.

3.3. Cyclic voltammetry (CV) test

Fig. 3 shows the typical cyclic voltammograms of different PbO_2 electrodes in 0.5 mol $\cdot L^{-1}$ Na_2SO_4 solution at the scan rate of 50 mV$\cdot s^{-1}$. As shown in Tab. 1, it could be seen that the oxygen evolution potential (OEP) of the unmodified PbO_2 electrode was 1.845 V. After the modification of PVA, the OEP increased for PbO_2-1.0 vt% (1.849 V) and PbO_2-2.0 vt% (1.862 V), respectively. However, when the volume fraction of PVA

reached to 5.0 vt%, the OEP decreased to 1.837 V. It was well accepted that electrodes with a high OEP were praised, because the oxygen evolution reaction and energy loss could be suppressed [10, 36, 37]. Therefore, this result implied that the PbO_2-2.0 vt% with the highest OEP could exhibit a better performances for organics removal than that of others.

In addition, the current response (at the section of oxygen evolution) of PbO_2-2.0 vt% was the most obvious. Xu et al. [38] considered that the high current response in the section of oxygen evolution could promote the water splitting and accelerate the generation rate of HO· free radical, which was also advantageous to the degradation of organic matter for PbO_2-2.0 vt%.

3.4. Electrochemical impedance spectroscopy (EIS)

Fig. 4 shows the EIS Nyquist plots of freshly prepared PbO_2 electrodes in 0.5 mol·L^{-1} Na_2SO_4 solutions and the simulated data is shown in Tab. 2. The Nyquist plots for all electrodes fit the equivalent circuit $R_s(R_fQ)$ very well. And R_s, R_f and Q represent the solution resistance, electrode film resistance and the constant phase element (CPE), respectively. From this figure, it could be seen that arc diameter of electrodes decreased with the increase of the volume fraction of PVA, revealing that the PVA addition could reduce the electrode film resistance and accelerate the electron transfer. As shown in Tab. 2, the PbO_2-2.0 vt% showed the smallest R_f (42.47 $\Omega \cdot cm^{-2}$), which was lower than that of PbO_2-0 vt% (102.1$\Omega \cdot cm^{-2}$). In addition, the PbO_2-2.0 vt% also showed the largest CPE value (0.000523 $\Omega^{-1} \cdot s^n \cdot cm^{-2}$) compared with other electrodes, reflecting a high specific area and more active sites on the electrode [39].

3.5. Electrochemical oxidation for ARG

Fig. 5 shows the performance of the PbO_2 electrodes for ARG degradation. From Fig. 5a, it could be clearly seen that the decolorization rates all reached more than 90% after 120 min electrolysis. The highest decolorization rate was obtained on PbO_2-2.0 vt% and decolorization rate could reach 89.3% within 60 min, which was higher than that of PbO_2-0 vt% (72.4%). After the kinetic fitting, we found that the removal of ARG was according to the first order kinetics (the inset). The rate constants (k) for PbO_2-0 vt%, PbO_2-1.0 vt%, PbO_2-2.0 vt% and PbO_2-5.0 vt% were $2.52 \times 10^{-2} \cdot min^{-1}$, $3.63 \times 10^{-2} \cdot min^{-1}$, $4.69 \times 10^{-2} \cdot min^{-1}$ and $2.87 \times 10^{-2} \cdot min^{-1}$, respectively. And the corresponding $t_{1/2}$ values were 33 min, 25 min, 23 min and 29 min, respectively (Tab. 3). As shown in Fig. 5b, the PbO_2-2.0 vt% possessed the highest COD removal rate value of 66.8% within 60 min, which was higher than that of others. Meanwhile, the PbO_2-2.0 vt% also showed the highest ICE (34.5%) and lowest E_p (0.041 $kWh \cdot gCOD^{-1}$) than those of the other PbO_2 electrodes. The best performance for ARG degradation at PbO_2-2.0 vt% could be ascribed to the high oxygen evolution potential, good electric conductivity and high specific area. These properties were helpful to generate more HO· free radicals and remove ARG at low energy consumption [40].

After ICP-AES detection, we found that the concentration of dissolved Pb element in the electrolyte decreased after the PVA modification (Tab. 4). This result could be explained as that after PVA modification, the morphology became smooth, compact and the grain sizes became smaller, which could slow down the erosion rate of electrolyte on the PbO_2 coating. As shown in Tab. 4, it could be seen that the

concentration of Pb element for PbO_2-0 vt%, PbO_2-1.0 vt%, PbO_2-2.0 vt% and

PbO_2-5.0 vt% were 0.023 mg $\cdot L^{-1}$, 0.011 mg $\cdot L^{-1}$, 0.006 mg $\cdot L^{-1}$ and 0.016 mg $\cdot L^{-1}$,

respectively. It could be observed that the PbO_2-2.0 vt% had the least amount of Pb

dissolution, implying the best safety performance in application.

3.6. X-ray photoelectron spectroscopy (XPS) analysis

In order to further explore the reasons for the good catalytic performance of PbO_2-2.0

vt% electrode, the XPS test was carried out for PbO_2-0 vt% and PbO_2-2.0 vt% (Fig. 6)

and XPS data of chemical states of O on the electrode surface is shown in Tab. 5. Fig.

6a shows the XPS whole spectra for PbO_2-0 vt% and PbO_2-2.0 vt%. From Fig. 6a, it

could be seen that the peaks of Pb, C and O existed in PbO_2-0 vt% electrode. As for

PbO_2-2.0 vt%, the peaks showed no obvious changes, indicating that the structure of

PbO_2 remained intact after PVA modification. From Fig. 6b and 6c, there existed two

types oxygen on the electrode surface. The peak at around 529 eV was attributed to

the lattice oxygen (O_L) and the peak at around 531 eV was attributed to adsorbed

hydroxyl oxygen (O_{ad}) [41]. As shown in Tab. 5, it could be observed that the percentage

of the O_{ad} to the total oxygen ($O_L + O_{ad}$) for PbO_2-2.0 vt% (76.81%) was higher than

that of PbO_2-0 vt% (68.95%). O_{ad} was the most active oxygen and could generate

more HO· free radicals, favoring the organics oxidation [42, 43]. Therefore, PbO_2-2.0 vt%

with a higher percentage of the O_{ad} implied a higher performance for ARG removal.

3.7. Electrochemical stability test.

Stability is an important index to evaluate the quality of electrodes. Therefore, the

stabilities of the PbO_2 electrodes were investigated through accelerated service life

tests (Fig. 7). It was clearly seen that the cell potential of the selected electrodes maintained relatively stable below the cell potential of around 4.0 V. Then the cell potential began to rise sharply in a short period of time, leading to deactivation. For PbO_2-1.0 vt% and PbO_2-2.0 vt%, the service life were 329.5 h and 256.5 h, respectively, which were higher than that of PbO_2-0 vt% (96 h). The enhancement of service life could be account for the smooth and compact morphology which could inhibit the infiltration of electrolyte into the coating and the formation of TiO_2 passivation layer. In addition, because of the improvement of oxygen evolution potential (OEP) for PbO_2-1.0 vt% and PbO_2-2.0 vt%, the diffusion of reactive oxygen species into the Ti substrate was also inhibited. Furthermore, the PVA addition could effectively reduce the internal stress of PbO_2 coating and improve the bonding strength between coating and substrate. For these reasons, the electrode stability had been greatly improved.

However, when the PVA volume fraction increased to 5.0 vt%, the service life decreased to 92.5 h, which was lower than that (96 h) of PbO_2-0 vt%. This result could be interpreted as that PVA addition could increase the viscosity of the electroplating solution and reduce the mass transfer rate of ions. Thus, when adding excess of PVA into the electroplating solution, the migration rate of Pb^{2+} ion to Ti/Sb-SnO_2 substrate would slow down and the average loading capacity of PbO_2 coating would decrease (only 83.5 mg·cm^{-2}) within a constant time. Therefore, the lower average loading capacity implied that the coating could be consumed in a relatively short period of time, leading to the deactivation of electrode rapidly.

Fig. 8 shows the SEM images and EDX spectrum of the deactivated PbO_2 electrodes From Fig. 8a and 8d, it could be seen that the PbO_2 coating still existed. However, compared with morphology of the fresh PbO_2-0 vt% and PbO_2-5.0 vt%, the typical rectangular pyramid structure of β-PbO_2 disappeared and the coating became very loose. After EDX analysis, it was found that there were still a large number of Pb element in the coating (Fig. 8e and 8h). This result indicated that the deactivation pattern of the two electrodes may be the substrate passivation. Although most of the PbO_2 surface coating still existed, the electrode was inactive. For PbO_2-1.0 vt% and PbO_2-2.0 vt%, the coating have been largely depleted and Ti substrate has been exposed. In addition, more Ti content was detected on the PbO_2-1.0 vt% and PbO_2-2.0 vt% after EDX analysis, which indicated that the depletion of the coating lead to the inactivation of PbO_2-1.0 vt% and PbO_2-2.0 vt%. It was known to all, the coating consumption was a much slower process than direct passivation of substrate[44]. Therefore, it could also explain the reason for the longer service life of PbO_2-1.0 vt% and PbO_2-2.0 vt% compared with PbO_2-0 vt% and PbO_2-5.0 vt%.

4. Conclusions

This study reported the preparation of PbO_2 electrode modified with polyvinyl alcohol (PVA) through electro-deposition technology. The results of SEM and XRD showed that the grain size of the modified electrode decreased and the morphology became compacted and smooth. The PVA addition could effectively improve the oxygen evolution potential (OEP) and reduce the electrode film resistance (R_f). This result showed that the PbO_2-2.0 vt% possessed the highest OEP (1.862 V) and lowest R_f

$(42.47 \ \Omega \cdot cm^{-2})$. From the electrochemical oxidation performances for ARG degradation, it could be seen that the PbO_2-2.0 vt% electrode showed the highest electrocatalytic activity for ARG degradation with the lowest energy consumption (E_p) due to its highest oxygen evolution potential (OEP), good electric conductivity and and massive O_{ad}. After the kinetic fitting, the removal of ARG was according to the first order kinetics and the rate constants (k) for PbO_2-2.0 vt% was $4.69 \times 10^{-2} \cdot min^{-1}$, which was 1.86 times higher than that of PbO_2-0 vt% ($2.52 \times 10^{-2} \cdot min^{-1}$). In addition, the dissolution reaction of Pb ion was suppressed after the PVA modification, ensuring the safety performance in application. Furthermore, the result of accelerated service life tests showed that the PbO_2-2.0 vt% electrode exhibited the highest stability and the accelerated service life was 329.5 h, which was more than 3 times longer than that of PbO_2-0 vt% electrode (96 h). Thus, the PbO_2-2.0 vt% electrode was considered to be the most optimal electrode in this study.

Acknowledgement

References

1.   Y. H. Cui, X. Y. Li and G. Chen, *Water research*, 2009, 43, 1968-1976.
2.   L. S. Andrade, T. T. Tasso, D. L. da Silva, R. C. Rocha-Filho, N. Bocchi and S. R. Biaggio, *Electrochimica Acta*, 2009, 54, 2024-2030.
3.   D. Li, J. Tang, X. Zhou, J. Li, X. Sun, J. Shen, LianjunWang and W. Han, *Chemosphere*, 2016, 149, 49-56.
4.   S. Chai, G. Zhao, Y. Wang, Y.-n. Zhang, Y. Wang, Y. Jin and X. Huang, *Applied Catalysis B: Environmental*, 2014, 147, 275-286.
5.   B. Cercado-Quezada, M.-L. Delia and A. Bergel, *Electrochemistry Communications*, 2011,

13, 440-443.

6.   A. N. Subba Rao and V. T. Venkatarangaiah, *Environmental science and pollution research international*, 2014, 21, 3197-3217.

7.   M. G. Tavares, L. V. A. da Silva, A. M. Sales Solano, J. Tonholo, C. A. Martínez-Huitle and C. L. P. S. Zanta, *Chemical Engineering Journal*, 2012, 204-206, 141-150.

8.   C. I. Brinzila, M. J. Pacheco, L. Ciríaco, R. C. Ciobanu and A. Lopes, *Chemical Engineering Journal*, 2012, 209, 54-61.

9.   W. Wu, Z.-H. Huang and T.-T. Lim, *Applied Catalysis A: General*, 2014, 480, 58-78.

10.   L. Zhang, L. Xu, J. He and J. Zhang, *Electrochimica Acta*, 2014, 117, 192-201.

11.   D. Devilliers and E. Mahé, *Electrochimica Acta*, 2010, 55, 8207-8214.

12.   I. Sirés, C. T. J. Low, C. Ponce-de-León and F. C. Walsh, *Electrochimica Acta*, 2010, 55, 2163-2172.

13.   X. Hao, Y. Quansheng, S. Dan, Y. Honghui, L. Jidong, F. Jiangtao and Y. Wei, *Journal of hazardous materials*, 2015, 286, 509-516.

14.   A. Y. Bagastyo, J. Radjenovic, Y. Mu, R. A. Rozendal, D. J. Batstone and K. Rabaey, *Water Res*, 2011, 45, 4951-4959.

15.   G. Zhao, Y. Zhang, Y. Lei, B. Lv, J. Gao, Y. Zhang and D. Li, *Environmental science & technology*, 2014, 44, 1754–1759.

16.   H. An, H. Cui, W. Zhang, J. Zhai, Y. Qian, X. Xie and Q. Li, *Chemical Engineering Journal*, 2012, 209, 86-93.

17.   J. Chen, Y. Xia and Q. Dai, *Electrochimica Acta*, 2015, 165, 277-287.

18.   C. Borrás, T. Laredo, J. Mostany and B. R. Scharifker, *Electrochimica Acta*, 2004, 49, 641-648.

19.   L. S. Andrade, R. C. Rocha-Filho, N. Bocchi, S. R. Biaggio, J. Iniesta, V. Garcia-Garcia and V. Montiel, *Journal of hazardous materials*, 2008, 153, 252-260.

20.   L. S. Andrade, L. A. Ruotolo, R. C. Rocha-Filho, N. Bocchi, S. R. Biaggio, J. Iniesta, V. Garcia-Garcia and V. Montiel, *Chemosphere*, 2007, 66, 2035-2043.

21.   Q. Li, Q. Zhang, H. Cui, L. Ding, Z. Wei and J. Zhai, *Chemical Engineering Journal*, 2013, 228, 806-814.

22.   X. Hao, S. Dan, Z. Qian, Y. Honghui and W. Yan, *RSC Advances*, 2014, 4, 25011.

23.   H. Kong, W. Li, H. Lin, Z. Shi, H. Lu, Y. Dan and W. Huang, *Surface and Interface Analysis*, 2013, 45, 715-721.

24.   J. Cao, H. Zhao, F. Cao and J. Zhang, *Electrochimica Acta*, 2007, 52, 7870-7876.

25.   H. Xu, Q. Zhang, W. Yan, W. Chu and L. Zhang, *International Journal of Electrochemical science* 2013, 8, 5382 - 5395.

26.   L. Aroui, L. Zerroual and M. Boutahala, *Materials Research Bulletin*, 2012, 47, 206-211.

27.   X. Duan, F. Ma, Z. Yuan, L. Chang and X. Jin, *Electrochimica Acta*, 2012, 76, 333-343.

28.   B. J. Hwang and K. L. Lee, *Journal of applied electrochemistry*, 1996, 26, 153-159.

29.   Q. Dai, H. Shen, Y. Xia, F. Chen, J. Wang and J. Chen, *Separation and Purification Technology*, 2013, 104, 9-16.

30.   X. Hao, G. Wuqi, W. Jia, F. Jiangtao, Y. Honghui and Y. Wei, *RSC Adv.*, 2016, 6, 7610-7617.

31.   W. H. Yang, W. T. Yang and X. Y. Lin, *Applied Surface Science*, 2012, 258, 5716-5722.

32.   C. C. DeMerlis and D. R. Schoneker, *FoodandChemical Toxicology*, 2003, 41, 319–326.

33.   S. Ghasemi, M. F. Mousavi and M. Shamsipur, *Electrochimica Acta*, 2007, 53, 459-467.

34.   X. Hu, R. Mamoto, Y. Shimomura, K. Kimbara and F. Kawai, *Archives of microbiology*, 2007, 188, 235-241.

35.   X. Li, D. Shao, H. Xu, W. Lv and W. Yan, *Chemical Engineering Journal*, 2016, 285, 1-10.

36.   Y. Chen, L. Hong, H. Xue, W. Han, L. Wang, X. Sun and J. Li, *Journal of Electroanalytical Chemistry*, 2010, 648, 119-127.

37.   Y. Yao, L. Cui, L. Jiao, X. Chen, N. Yu and H. Dong, *Journal of Solid State Electrochemistry*, 2015, 20, 725-731.

38.   L. Xu, M. Li and W. Xu, *Electrochimica Acta*, 2015, 166, 64-72.

39.   D. Shao, W. Yan, X. Li and H. Xu, *ACS Sustainable Chemistry & Engineering*, 2015, 3, 1777-1785.

40.   S.-P. Tong, C.-A. Ma and H. Feng, *Electrochimica Acta*, 2008, 53, 3002-3006.

41.   Y. Duan, Q. Wen, Y. Chen, T. Duan and Y. Zhou, *Applied Surface Science*, 2014, 320, 746-755.

42.   S. Yang, Y. Feng, J. Wan, W. Zhu and Z. Jiang, *Applied Surface Science*, 2005, 246, 222-228.

43.   N. K. V. Leitner and M. Dope, *Water Reserch*, 1996, 31, 1383–1397.

44.   D. Shao, W. Yan, X. Li, H. Yang and H. Xu, *Industrial & Engineering Chemistry Research*, 2014, 53, 3898-3907.

Figure captions

Fig. 1. SEM images of the different PbO_2 electrodes (a: PbO_2-0 vt%, b: PbO_2-1.0 vt%, c: PbO_2-2.0 vt%, d: PbO_2-5.0 vt%).

Fig. 2. XRD patterns of the different PbO_2 electrodes.

Fig. 3. Cyclic voltammograms curves of PbO_2 electrodes in 0.5 mol $\cdot L^{-1}$ Na_2SO_4 solution, scan rate: 50 mV$\cdot s^{-1}$.

Fig. 4. The fitted curves of PbO_2 electrodes in EIS and equivalent circuit model (the inset).

Fig. 5. Performance of the PbO_2 electrodes for ARG degradation. (a) ARG decolorization rate; (b) COD removal rate.

Fig. 6. XPS spectra of PbO_2 electrode PbO_2-0 vt% and PbO_2-2.0 vt%. (a) XPS fully scanned spectra; (b) O 1s core level spectrum for PbO_2-0 vt%; (d) O 1s core level spectrum for PbO_2-2.0 vt%.

Fig. 7. Accelerated life test of selected PbO_2 electrodes (H_2SO_4: 3 mol$\cdot L^{-1}$; current density: 500 mA$\cdot cm^{-2}$).

Fig. 8. SEM images and EDX spectrum of the deactivated PbO_2-0 vt% electrode (a, e), PbO_2-1.0 vt% (b, f), PbO_2-2.0 vt% (c, g) and PbO_2-5.0 vt% (d, h).
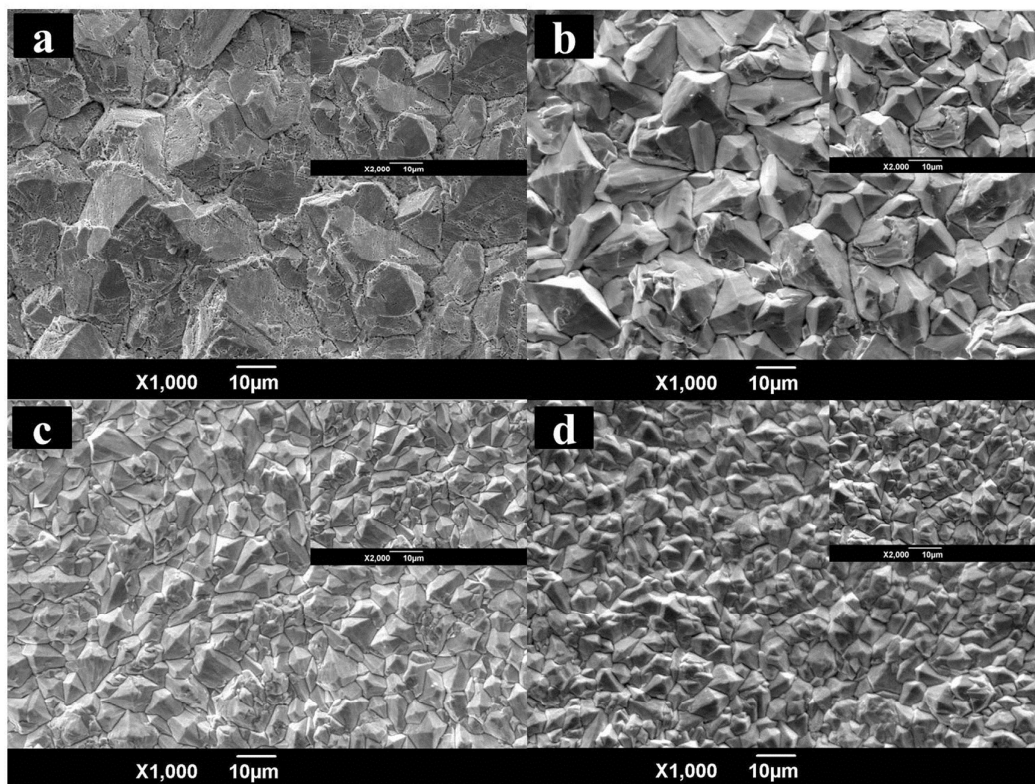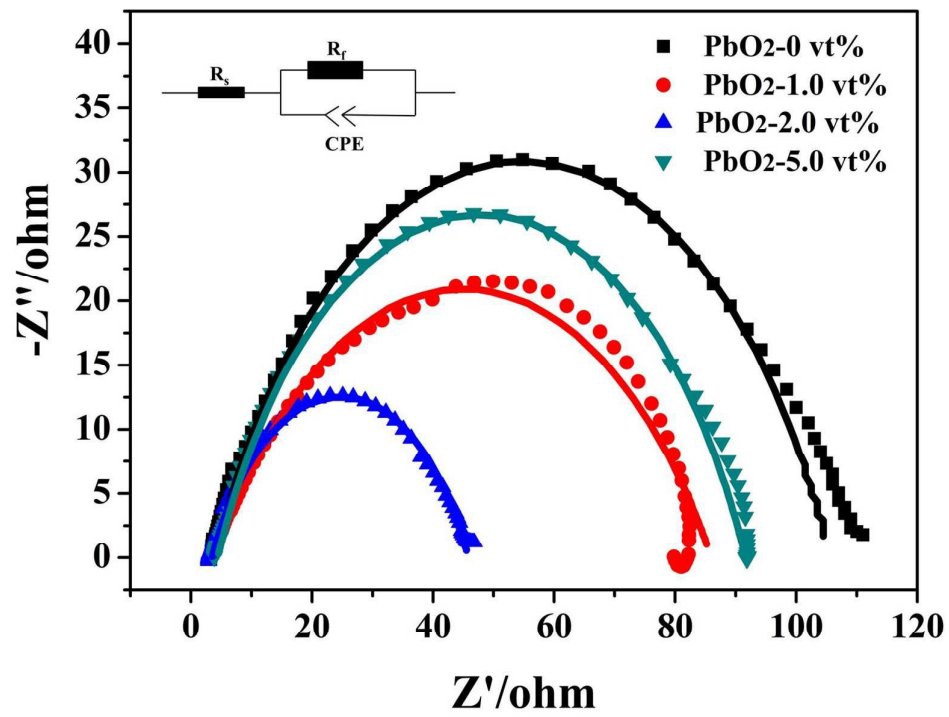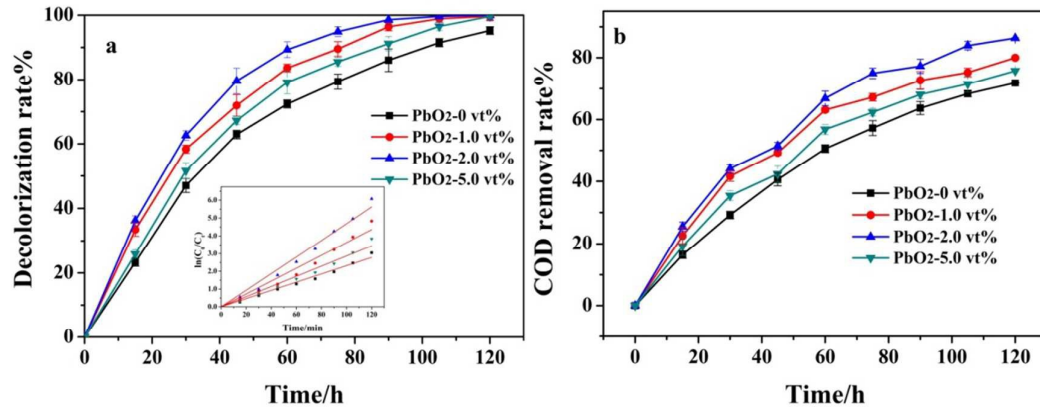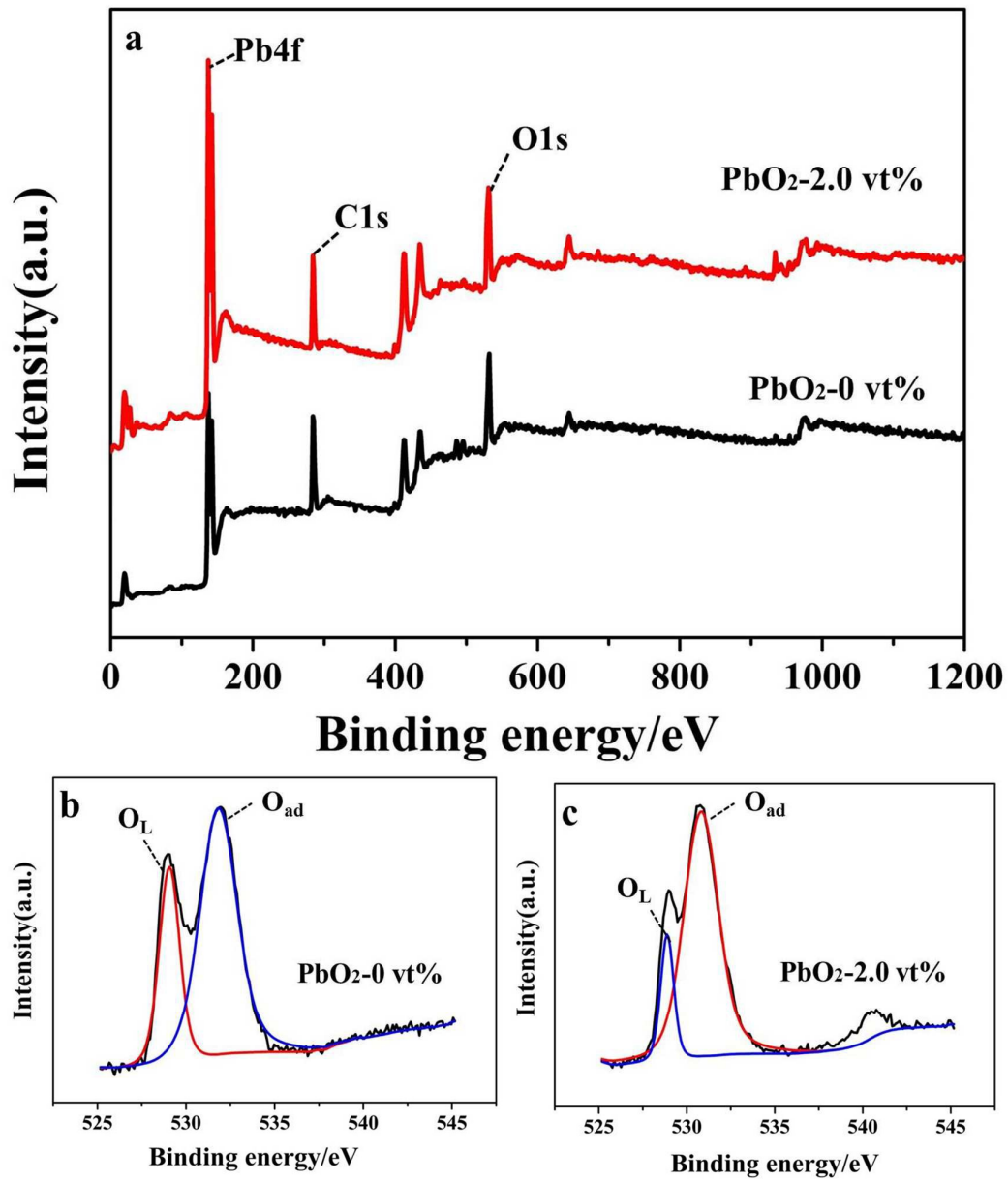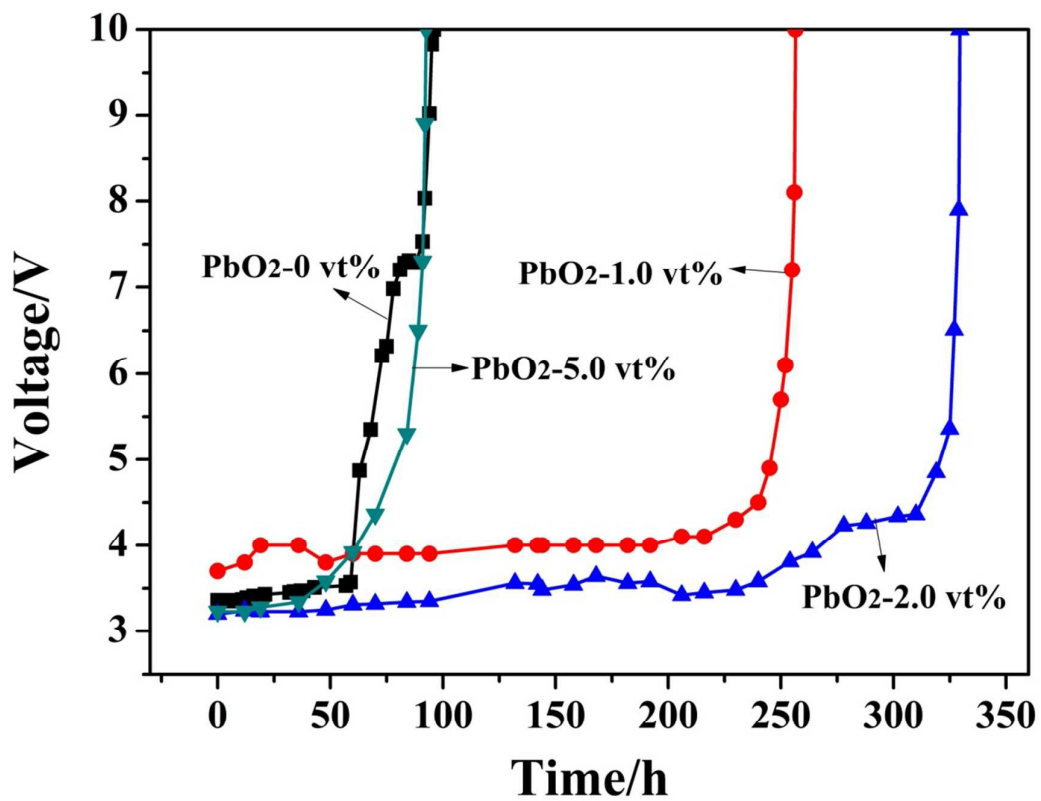
Fig. 1
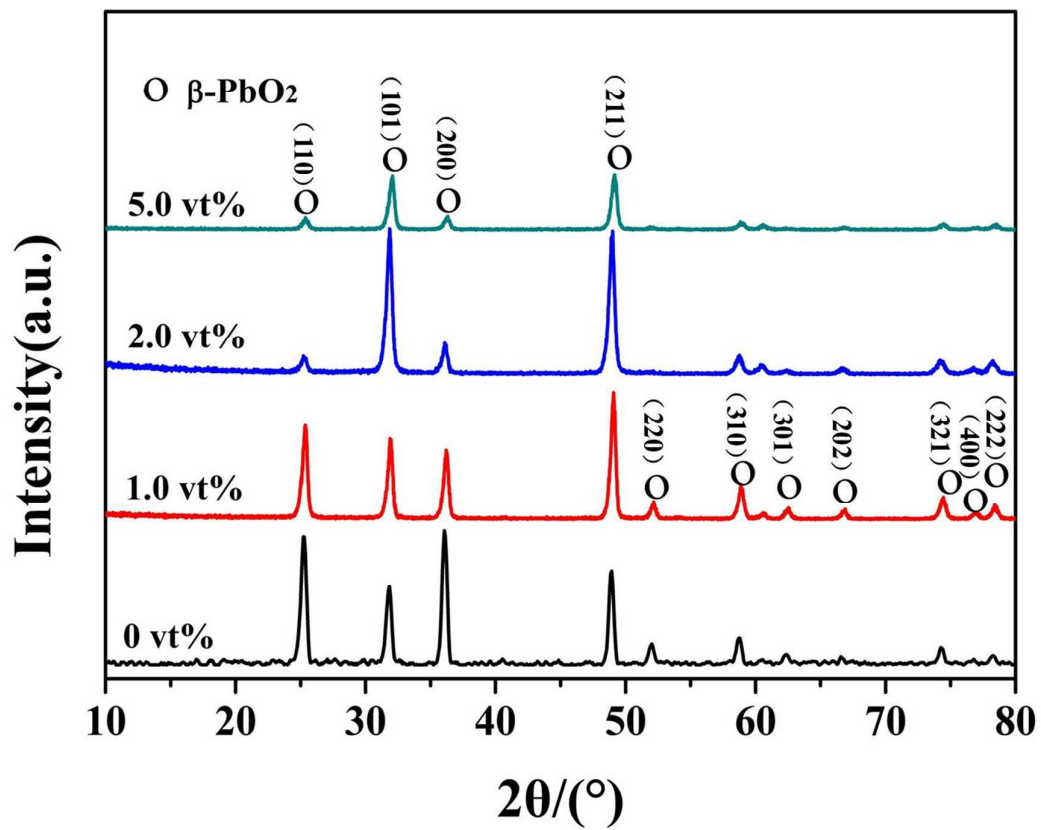
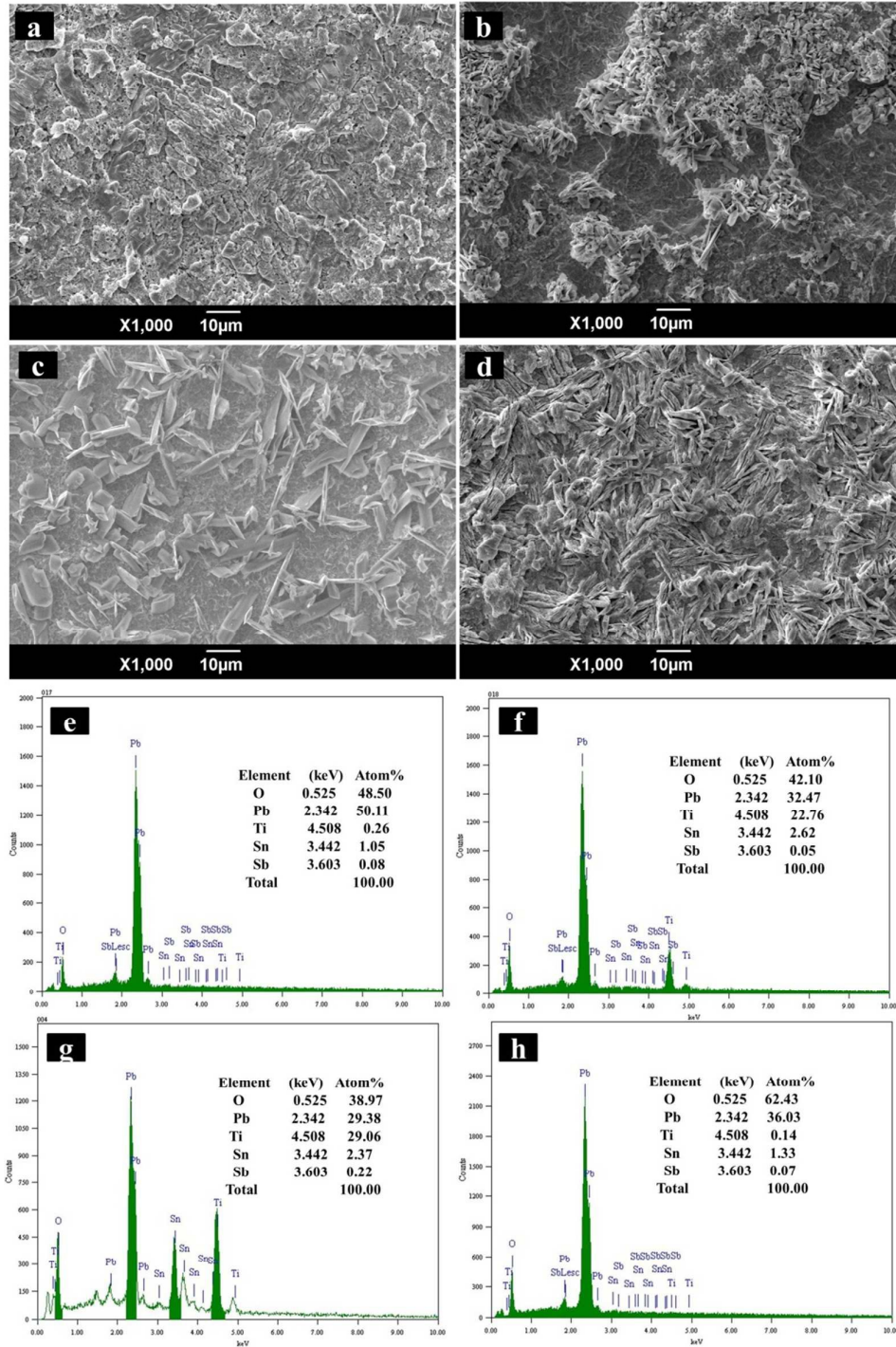Fig. 2
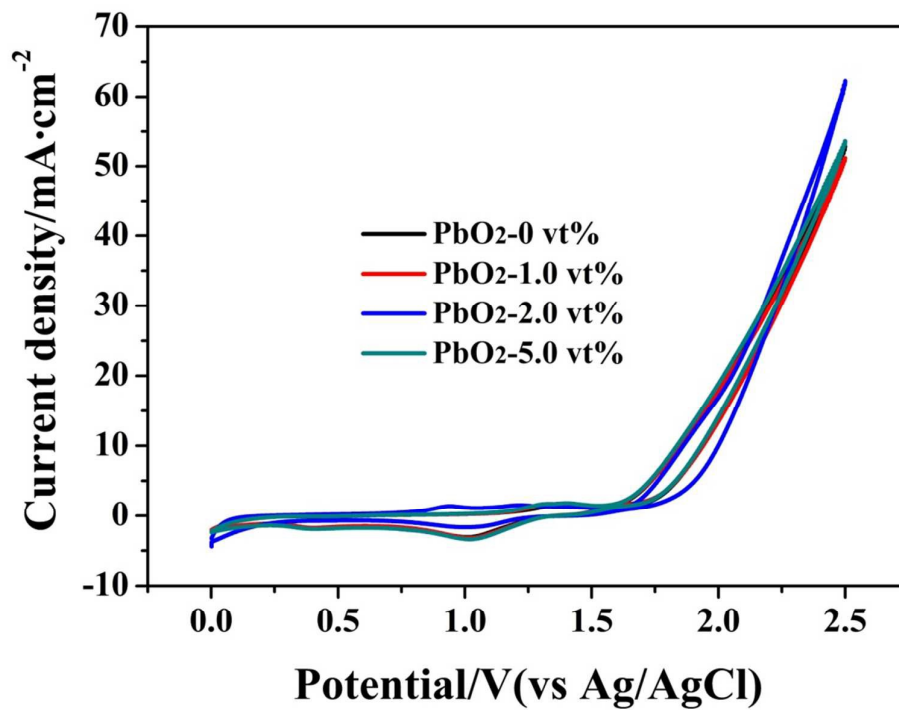
Fig. 3

Fig. 4

Fig. 5

Fig. 6

Fig. 7

Fig. 8

Table captions

Tab. 1. The different parameters of selected PbO_2 electrodes.

Tab. 2. Simulated data of each parameter (EIS).

Tab. 3. The kinetics for the electrochemical degradation of ARG (electrolysis time:

120 min).

Tab. 4. The concentration of Pb element in the electrolyte (electrolysis time: 120 min).

Tab. 5. XPS data of chemical states of O on the electrode surface.

Tab. 1

	PbO_2-0 vt%	PbO_2-1.0 vt%	PbO_2-2.0 vt%	PbO_2-5.0 vt%
Average loading capacity/mg·cm^{-2}	91.9	91.6	91.3	83.5
Grain size/nm	21.2	20.9	19.3	19.1
OEP/V	1.845	1.849	1.862	1.837
Accelerated lifetime/h	96	256.5	329.5	92.5

OEP represents oxygen evolution potential

Tab. 2

	$R_s/\Omega \cdot cm^{-2}$	$R_f/\Omega \cdot cm^{-2}$	$Q/\Omega^{-1} \cdot s^n \cdot cm^{-2}$	n
PbO_2-0 vt%	3.272	102.1	0.000245	0.695
PbO_2-1.0 vt%	3.410	82.21	0.000262	0.601
PbO_2-2.0 vt%	2.909	42.47	0.000523	0.684
PbO_2-5.0 vt%	3.821	87.39	0.000191	0.701

Tab. 3

Electrode	Rate constants $(k, 10^{-2}\,\text{min}^{-1})^{a}$	Half-lives $(t_{1/2}, \text{min})$	R^2	ICE $(\%)^{b}$	E_p $(\text{kWh}\cdot\text{gCOD}^{-1})^{c}$
PbO$_2$-0 vt%	2.52	33	0.991	24.8	0.057
PbO$_2$-1.0 vt%	3.63	25	0.993	32.0	0.044
PbO$_2$-2.0 vt%	4.69	23	0.990	34.5	0.041
PbO$_2$-5.0 vt%	2.87	29	0.988	28.1	0.050

[a] Pseudo-first-order rate constant of electrochemical degradation

[b,c] The values of ICE and E_p were both obtained at the time of 50% COD removal

Tab. 4

Electrode	PbO$_2$-0 vt%	PbO$_2$-1.0 vt%	PbO$_2$-2.0 vt%	PbO$_2$-5.0 vt%
Concentration (mg·L^{-1})	0.023	0.011	0.006	0.016

Tab. 5

Electrode	Binding energy (eV)		$\varepsilon\%$	η
	O1s (O_L)	O1s (O_{ad})	$O_{ad}/(O_{ad}+O_L)100\%$	(O_{ad}/O_L)
PbO_2-0 vt%	529.06	531.82	68.95	2.22
PbO_2-2 vt%	529.01	531.02	76.81	3.31

O_{ad}: adsorbed hydroxyl oxygen;

O_L: lattice oxygen.